

Automatic Search Interval for Smoothing Parameter in Penalized Splines

Zheyuan Li¹ and Jiguo Cao^{2*}

¹School of Mathematics and Statistics, Henan University, Kaifeng, Henan, China.

²Department of Statistics and Actuarial Science, Simon Fraser University, Burnaby, British Columbia, Canada.

*Corresponding author(s). E-mail(s): jiguo_cao@sfu.ca;

Contributing authors: zheyuan.li@vip.henu.edu.cn;

Abstract

The selection of smoothing parameter is central to estimation of penalized splines. The best parameter value is often the one that optimizes a smoothness selection criterion, like the minimizer of generalized cross-validation error (GCV) and the maximizer of restricted likelihood (REML). To avoid ending up with an undesired local extremum rather than the global extremum, grid search should be used for optimization. Unfortunately, the method requires a pre-specified search interval that contains the unknown global extremum and there has not been any theory on how it could be provided. As a result, practitioners have to find it by trial and error. To overcome such difficulty, we develop novel algorithms to automatically find this interval. Our automatic search interval has four advantages. (i) It specifies a smoothing parameter range where the penalized least squares problem is numerically solvable. (ii) It is criterion-independent, so that different criteria like GCV and REML can be explored on the same parameter range. (iii) It is sufficiently wide to contain the global extremum of any criterion, so that for example, the global minimum of GCV and the global maximum of REML can both be identified. (iv) It is computationally cheap compared with grid search so that it carries no extra costs in practice. Our method is ready to use through **R** package **gps** (\geq version 1.1). It may be embedded in other advanced statistical modeling methods that rely on penalized splines.

Keywords: grid search, O-splines, penalized B-splines, P-splines

1 Introduction

Penalized splines are flexible methods for smooth function estimation. They have been applied in many statistical modeling frameworks, including generalized additive models (Spiegel et al, 2019), single-index models (Wang et al, 2018), generalized partially linear single-index models (Yu et al, 2017), functional mixed-effects models (Chen et al, 2018), survival models (Orbe and Virto, 2021;

Bremhorst and Lambert, 2016), models for longitudinal data (Koehler et al, 2017; Andrinopoulou et al, 2018), additive quantile regression models (Muggeo et al, 2021), varying coefficient models (Hendrickx et al, 2018), quantile varying coefficient models (Gijbels et al, 2018), spatial models (Greco et al, 2018; Rodriguez-Alvarez et al, 2018), spatiotemporal models (Minguez et al, 2020; Goicoa et al, 2019) and spatiotemporal quantile or

expectile regression models (Franco-Villoria et al, 2019; Spiegel et al, 2020).

To explain the fundamental idea of a penalized spline, consider a smoothing model for $(x_i, y_i)_1^n$:

$$y_i = f(x_i) + e_i, \quad e_i \stackrel{\text{iid}}{\sim} N(0, \sigma_e^2).$$

We set up $f(x) = \sum_{j=1}^p \mathcal{B}_j(x) \beta_j$ with some spline basis $(\mathcal{B}_j(x))_1^p$ and estimate $\beta = (\beta_1, \beta_2, \dots, \beta_p)^T$ by minimizing the penalized least squares (PLS):

$$\|\mathbf{y} - \mathbf{B}\beta\|^2 + c^\rho \beta^T \mathbf{S}\beta, \quad (1)$$

where \mathbf{B} is a design matrix with element $B_{ij} = \mathcal{B}_j(x_i)$ and $\mathbf{y} = (y_1, y_2, \dots, y_n)^T$. With a sensible construction of \mathbf{S} , the penalty term $\beta^T \mathbf{S}\beta$ is a wiggleness measure for $f(x)$ and $\rho \in (-\infty, +\infty)$ is a smoothing parameter that trades off $f(x)$'s closeness to data for its smoothness. The choice of ρ is critical and it is often selected by minimizing generalized cross-validation error (GCV) (Wahba, 1990) or maximizing restricted likelihood (REML) (Wood, 2017). Many strategies can be applied to this one-dimensional optimization, but to avoid getting an undesired local extremum rather than the global extremum, grid search should be used. Specifically, we attempt a grid of ρ values in a search interval $[\rho_{\min}, \rho_{\max}]$ and pick the value that optimizes the criterion.

To illustrate that a criterion can have multiple local extrema and mistaking a local extremum for the global extremum leads to undesirable result, consider smoothing daily new deaths attributed to COVID-19 in Finland from 2020-09-01 to 2022-03-01 and daily new confirmed cases of COVID-19 in Netherlands from 2021-09-01 to 2022-03-01 (data source: Our World in Data (Ritchie et al, 2020)). Figure 1 shows that the GCV error (against ρ) in each example has a local minimum and a global minimum. The fitted spline corresponding to the local minimum is wiggly (especially for Finland), whereas the fit corresponding to global minimum is smoother and more plausible. In particular, the smooth fit reasonably depicts the single bulge in the Omicron wave for Netherlands. In both cases, minimizing GCV via gradient descent or Newton's method can be trapped in the local minimum, if the initial guess of ρ is in its neighborhood. By contrast, grid search for ρ values in $[-6, 5]$ (as the Figure shows) finds the global minimum.

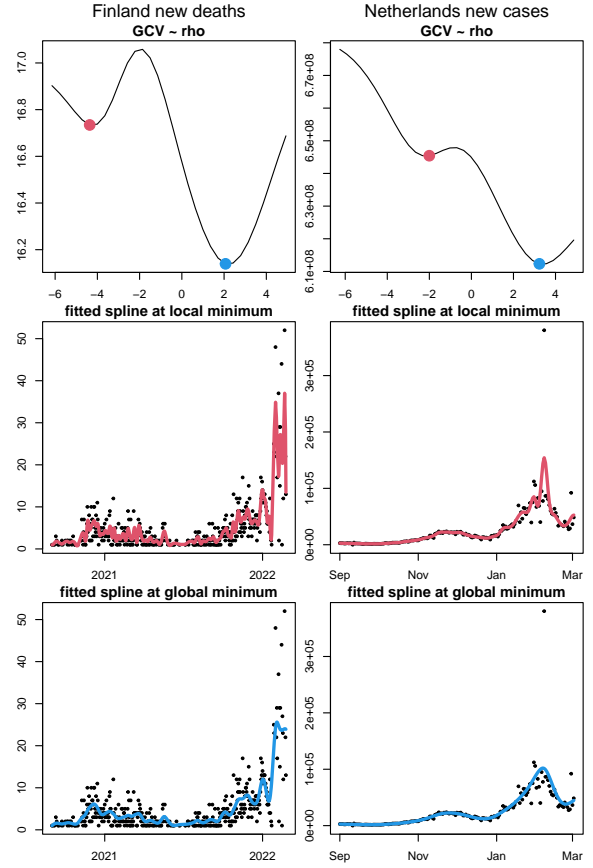


Fig. 1 A smoothness selection criterion can have multiple extrema and mistaking a local extremum for the global extremum leads to undesirable fit. Row 1: GCV error has a local minimum (red) and a global minimum (blue). Row 2: The fitted spline corresponding to the local minimum is wiggly. Row 3: The fit corresponding to global minimum is smoother and more plausible. Both examples come from daily COVID-19 data smoothing. Left column: new deaths in Finland from 2020-09-01 to 2022-03-01; Right column: new cases in Netherlands from 2021-09-01 to 2022-03-01.

In general, to successfully identify the global extremum of a criterion function in grid search, the search interval $[\rho_{\min}, \rho_{\max}]$ must be sufficiently wide so that the criterion can be fully explored. Unfortunately, there has not been any theory on how to provide this interval, so practitioners have to find it by trial and error. This inevitably causes two problems. First of all, the PLS problem (1) is not numerically solvable for a ρ value too large, because the resulting linear system for β will be rank-deficient. A ρ value too small triggers the same problem if $p > n$, because the unpenalized regression spline problem has no unique solution. As a result, practitioners do not even know what

ρ range is numerically safe to attempt. Secondly, a PLS solver is often a computational kernel for more advanced smoothing problems, like robust smoothing with M-estimators (Dreassi et al, 2014; Osorio, 2016) and backfitting-based generalized additive models (Eilers and Marx, 2002; Oliveira and Paula, 2021; Hernando Vanegas and Paula, 2016). In these problems, a PLS needs be solved in each iteration for reweighted data and it is more difficult to pre-specify a search interval because it changes from iteration to iteration.

To resolve these issues, we develop algorithms to automatically find an appropriate $[\rho_{\min}, \rho_{\max}]$ for grid search. Our automatic search interval has four advantages. (i) It gives a safe ρ range where the PLS problem (1) is numerically solvable. (ii) It is criterion-independent so that different criteria, including GCV and REML, can be explored on the same ρ range. (iii) It is wide enough to contain the global extremum of any smoothness selection criterion, so that for example, the global minimum of GCV and the global maximum of REML can both be identified. (iv) It is computationally cheap compared with grid search, so in practice it carries no extra costs.

The rest of this paper derives and illustrates automatic search intervals for ρ (Sections 2 and 3), conducts simulation studies on these intervals (Section 4) and revisits the COVID-19 example in greater depth (Section 5). We will introduce our method using penalized B-splines, because it is particularly challenging to develop algorithms for this subclass of penalized splines to achieve (iv). We will describe how to adapt our method for other types of penalized splines in the end of this paper. Our method is ready to use via **R** package **gps** (\geq version 1.1) (Li and Cao, 2022b). It may be embedded in other advanced statistical modeling methods that rely on penalized splines.

2 Penalized B-Splines

There exists a wide variety of penalized splines, depending on the exact choice of basis and penalty. Examples include natural cubic spline basis with a derivative penalty (Wood, 2017, section 5.3.1), thin-plate spline basis with a derivative penalty (Wood, 2017, section 5.5.1), truncated power basis with a ridge penalty (Ruppert et al, 2003) and the penalized B-splines family, i.e., B-splines (de Boor, 2001) with a derivative or difference penalty. See

Li and Cao (2022a) for an excellent description of this family. For this family, the PLS objective can be expressed as:

$$\|\mathbf{y} - \mathbf{B}\boldsymbol{\beta}\|^2 + e^\rho \|\mathbf{D}_m \boldsymbol{\beta}\|^2, \quad (2)$$

where $\mathbf{S} = \mathbf{D}_m^\top \mathbf{D}_m$ in connection with (1). Family members differ in the type of knots underlying the $n \times p$ B-spline design matrix \mathbf{B} , as well as the $(p - m) \times p$ matrix \mathbf{D}_m applied to B-spline coefficients $\boldsymbol{\beta}$. Standard P-splines (Eilers and Marx, 1996) are tailored for B-splines on equidistant knots, while O-splines (O’Sullivan, 1986) and general P-splines (Li and Cao, 2022a) also accommodate B-splines on unevenly spaced knots. As for \mathbf{D}_m , standard and general P-splines use a standard and general difference matrix, respectively, while O-splines use a matrix associated with a derivative penalty that penalizes $\int f^{(m)}(x)^2 dx$. In general, we can define \mathbf{B} for B-splines of order $d \geq 2$ and \mathbf{D}_m for penalty order $1 \leq m \leq d - 1$. See Appendix A for concrete examples. In practice, \mathbf{D}_m can be conveniently computed by function **SparseD** from package **gps**.

Now, given a ρ value, the solution to (2) is:

$$\hat{\boldsymbol{\beta}} = \mathbf{C}^{-1} \mathbf{B}^\top \mathbf{y},$$

where $\mathbf{C} = \mathbf{B}^\top \mathbf{B} + e^\rho \mathbf{D}_m^\top \mathbf{D}_m$ is $p \times p$ symmetric. The fitted values $\hat{\mathbf{y}} = (\hat{y}_1, \hat{y}_2, \dots, \hat{y}_n)^\top$ are:

$$\hat{\mathbf{y}} = \mathbf{B} \hat{\boldsymbol{\beta}} = \mathbf{B} \mathbf{C}^{-1} \mathbf{B}^\top \mathbf{y}.$$

The complexity of the fitted spline is measured by its effective degree of freedom (edf), defined as the trace of the hat matrix that maps \mathbf{y} to $\hat{\mathbf{y}}$:

$$\text{edf}(\rho) = \text{tr}(\mathbf{B} \mathbf{C}^{-1} \mathbf{B}^\top) = \text{tr}(\mathbf{C}^{-1} \mathbf{B}^\top \mathbf{B}).$$

Note that edf is a function of ρ , which explains why the choice of ρ affects the resulting fit. It also depends on \mathbf{B} (basis) and \mathbf{D}_m (penalty), but be aware that it does not depend on \mathbf{y} .

An advantage of penalized B-splines over other types of penalized splines, is their computational efficiency. It is known that computing \mathbf{C}^{-1} costs $O(p^3)$ floating point operations when \mathbf{C} is a dense matrix. However, for penalized B-splines, $\mathbf{B}^\top \mathbf{B}$, $\mathbf{D}_m^\top \mathbf{D}_m$ and hence \mathbf{C} are sparse band matrices. As a result, computational complexity for a given ρ is only $O(p^2)$. Note that we don’t explicitly form this inverse matrix. Rather, we compute the Cholesky

factorization $\mathbf{C} = \mathbf{K}\mathbf{K}^T$ for the lower triangular matrix \mathbf{K} (which inherits \mathbf{C} 's band sparsity), then obtain $\hat{\beta}$ by solving two triangular band systems with respect to \mathbf{K} and \mathbf{K}^T . The edf can also be calculated at $O(p^2)$ costs. To see this, let's first compute the Cholesky factorization (which only needs be done once as it does not depend on ρ) $\mathbf{B}^T\mathbf{B} = \mathbf{L}\mathbf{L}^T$, where \mathbf{L} is a lower triangular band matrix. Then together with the factorization of \mathbf{C} , we can show:

$$\begin{aligned} \text{edf}(\rho) &= \text{tr}(\mathbf{C}^{-1}\mathbf{L}\mathbf{L}^T) = \text{tr}(\mathbf{L}^T\mathbf{C}^{-1}\mathbf{L}) \\ &= \text{tr}((\mathbf{K}^{-1}\mathbf{L})^T\mathbf{K}^{-1}\mathbf{L}) = \|\mathbf{K}^{-1}\mathbf{L}\|_F^2. \end{aligned} \quad (3)$$

Here, $\|\mathbf{X}\|_F^2$ denotes the squared Frobenius norm of \mathbf{X} , which is simply the sum of squared matrix elements. Again, we don't form the inverse matrix, but solve the triangular band system $\mathbf{K}\mathbf{X} = \mathbf{L}$. Once the edf is obtained, it is trivial to calculate the GCV error:

$$\text{GCV}(\rho) = \frac{n\|\mathbf{y} - \hat{\mathbf{y}}\|^2}{(n - \text{edf})^2}.$$

The restricted likelihood REML(ρ) has a more complicated form and is detailed in Appendix B. In short, solving PLS for a given ρ value involves $O(p^2)$ costs. When ρ is selected via a grid search over N trial values to minimize GCV or maximize REML, the overall computational costs is $O(Np^2)$.

Note that to compute \mathbf{L} , the design matrix \mathbf{B} must have full column rank, which requires $p < n$. This is often satisfied in practice and with fewer B-splines than data, a penalized spline is a low-rank estimator. This condition is also a prerequisite for the upcoming method for finding automatic search intervals, as \mathbf{L} is an indispensable quantity.

3 Automatic Search Interval

3.1 An Exact Search Interval

We start with an alternative way to compute edf. By forming the $p \times q$ matrix (at $O(p^2)$ costs):

$$\mathbf{E} = \mathbf{L}^{-1}\mathbf{D}_m^T, \quad (4)$$

we can express \mathbf{C} as:

$$\begin{aligned} \mathbf{C} &= \mathbf{L}\mathbf{L}^T + e^\rho\mathbf{D}_m^T\mathbf{D}_m \\ &= \mathbf{L}[\mathbf{I} + e^\rho\mathbf{E}\mathbf{E}^T]\mathbf{L}^T. \end{aligned} \quad (5)$$

Plugging this into $\text{edf}(\rho) = \text{tr}(\mathbf{L}^T\mathbf{C}^{-1}\mathbf{L})$ (see (3)), we get:

$$\text{edf}(\rho) = \text{tr}([\mathbf{I} + e^\rho\mathbf{E}\mathbf{E}^T]^{-1}),$$

where \mathbf{I} is an identity matrix. The $p \times p$ symmetric matrix $\mathbf{E}\mathbf{E}^T$ is positive semi-definite with rank $q = p - m$, so it has q positive eigenvalues $\lambda_1 > \lambda_2 > \dots > \lambda_q$ followed by m zero eigenvalues. Let its eigendecomposition be $\mathbf{E}\mathbf{E}^T = \mathbf{U}\mathbf{\Lambda}\mathbf{U}^{-1}$, where \mathbf{U} is an orthonormal matrix with eigenvectors and $\mathbf{\Lambda}$ is a $p \times p$ diagonal matrix with eigenvalues, then:

$$\begin{aligned} \text{edf}(\rho) &= \text{tr}([\mathbf{U}\mathbf{U}^{-1} + e^\rho\mathbf{U}\mathbf{\Lambda}\mathbf{U}^{-1}]^{-1}) \\ &= \text{tr}([\mathbf{U}(\mathbf{I} + e^\rho\mathbf{\Lambda})\mathbf{U}^{-1}]^{-1}) \\ &= \text{tr}(\mathbf{U}(\mathbf{I} + e^\rho\mathbf{\Lambda})^{-1}\mathbf{U}^{-1}) \\ &= \text{tr}((\mathbf{I} + e^\rho\mathbf{\Lambda})^{-1}) \\ &= m + \sum_{j=1}^q (1 + e^\rho\lambda_j)^{-1}. \end{aligned}$$

We call $(\lambda_j)_1^q$ the Demmler-Reinsch eigenvalues, in tribute to [Demmler and Reinsch \(1975\)](#) who first studied the eigenvalue problem of smoothing splines ([Reinsch, 1967, 1971](#)). We also define

$$\text{redf}(\rho) = \sum_{j=1}^q \frac{1}{1 + e^\rho\lambda_j} \quad (6)$$

as the restricted edf. The result shows that redf is a monotonically decreasing function of ρ . As $\rho \rightarrow -\infty$, redf increases to q . As $\rho \rightarrow +\infty$, redf decreases to 0. Given this one-to-one matching between ρ and redf, it is clear that choosing the optimal ρ is equivalent to choosing the optimal redf. Such observation is enlightening. While it is difficult to see what $[\rho_{\min}, \rho_{\max}]$ is wide enough for grid search, it is easy to see what $[\text{redf}_{\min}, \text{redf}_{\max}]$ is adequate. For example,

$$\begin{aligned} \text{redf}_{\min} &= q\kappa, \\ \text{redf}_{\max} &= q(1 - \kappa), \end{aligned} \quad (7)$$

with a small κ are reasonable. We interpret κ as a coverage parameter as $[\text{redf}_{\min}, \text{redf}_{\max}]$ covers $1 - 2\kappa$ of $[0, q]$. In practice, $\kappa = 0.01$ is good enough, in which case, $[\text{redf}_{\min}, \text{redf}_{\max}]$ covers 98% of $[0, q]$. It then follows that ρ_{\min} and ρ_{\max} satisfy

$$\begin{aligned} \text{redf}(\rho_{\min}) &= \text{redf}_{\max}, \\ \text{redf}(\rho_{\max}) &= \text{redf}_{\min}, \end{aligned} \quad (8)$$

and can be solved for via root-finding. As $\text{redf}(\rho)$ is differentiable, we may use Newton's method for this task. See Algorithm 1 for an implementation for a general root-finding problem $g(x) = 0$.

Algorithm 1 Newton's method for finding root of $g(x) = 0$. Input: (i) x , an initial value, (ii) δ_{\max} , maximum size of a Newton step.

```

1:  $g = g(x)$ 
2: loop
3:    $g' = g'(x)$ 
4:    $\delta = -g'/g$ 
5:   if  $|\delta| < |g|10^{-6}$  then
6:     break
7:   end if
8:    $\delta = \text{sign}(\delta) \cdot \min(|\delta|, \delta_{\max})$ 
9:   loop
10:     $\tilde{x} = x + \delta_k$ 
11:     $\tilde{g} = g(\tilde{x})$ 
12:    if  $|\tilde{g}| < |g|$  then
13:      break
14:    end if
15:     $\delta = \delta/2$ 
16:  end loop
17:   $x = \tilde{x}$ 
18:   $g = \tilde{g}$ 
19: end loop
20: return  $x$ 

```

Note that the search interval $[\rho_{\min}, \rho_{\max}]$ is purely derived from redf . As redf does not depend on y values or smoothness selection criteria, the interval depends on neither y values nor criteria. This is a nice property and an advantage of our method. We call this novel idea the redf -oriented thinking, contrary to the convention which finds a new interval whenever y values or criterion change.

However, the interval comes with a downside. It is computationally expensive due to the $O(p^3)$ costs in the eigendecomposition for $(\lambda_j)_1^q$. Section 2 shows that solving PLS along with grid search only involves $O(Np^2)$ complexity, so when p is big, finding the interval is even more costly than the subsequent grid search. This is unacceptable and we need a better strategy.

3.2 A Wider Search Interval

In fact, we don't have to find the exact $[\rho_{\min}, \rho_{\max}]$ that satisfies (7) and (8). It suffices to find a wider

interval

$$[\rho_{\min}^*, \rho_{\max}^*] \supseteq [\rho_{\min}, \rho_{\max}].$$

That is, we find ρ_{\min}^* and ρ_{\max}^* such that $\rho_{\min} \geq \rho_{\min}^*$ and $\rho_{\max} \leq \rho_{\max}^*$. Surprisingly, in this way, we only need the maximum eigenvalue λ_1 and the minimum eigenvalue λ_q , instead of all eigenvalues $(\lambda_j)_1^q$. To see this, note that $\lambda_1 \geq \lambda_j \geq \lambda_q$ implies:

$$\sum_{j=1}^q \frac{1}{1 + e^{\rho} \lambda_1} \leq \sum_{j=1}^q \frac{1}{1 + e^{\rho} \lambda_j} \leq \sum_{j=1}^q \frac{1}{1 + e^{\rho} \lambda_q},$$

hence,

$$\frac{q}{1 + e^{\rho} \lambda_1} \leq \text{redf}(\rho) \leq \frac{q}{1 + e^{\rho} \lambda_q}.$$

Since the result holds for any ρ , including ρ_{\min} and ρ_{\max} , we have:

$$\begin{aligned} \text{redf}(\rho_{\min}) &\geq \frac{q}{1 + e^{\rho_{\min}} \lambda_1}, \\ \text{redf}(\rho_{\max}) &\leq \frac{q}{1 + e^{\rho_{\max}} \lambda_q}. \end{aligned}$$

Together with (7) and (8), we see:

$$\begin{aligned} q(1 - \kappa) &\geq \frac{q}{1 + e^{\rho_{\min}} \lambda_1}, \\ q\kappa &\leq \frac{q}{1 + e^{\rho_{\max}} \lambda_q}. \end{aligned}$$

These imply:

$$\begin{aligned} \rho_{\min} &\geq \overbrace{\log \left(\frac{\kappa}{(1 - \kappa) \lambda_1} \right)}^{\rho_{\min}^*}, \\ \rho_{\max} &\leq \underbrace{\log \left(\frac{1 - \kappa}{\kappa \lambda_q} \right)}_{\rho_{\max}^*}. \end{aligned}$$

Actually, we can replace the maximum eigenvalue λ_1 by the mean eigenvalue $\bar{\lambda} = \sum_{j=1}^q \lambda_j / q$ for a tighter lower bound. To see this, recall that the harmonic mean of positive numbers $(a_j)_1^q$ is no larger than their arithmetic mean, i.e.,

$$\frac{q}{\sum_{j=1}^q \frac{1}{a_j}} \leq \bar{a} \Rightarrow \frac{q}{\bar{a}} \leq \sum_{j=1}^q \frac{1}{a_j}.$$

Setting $a_j = 1 + e^\rho \lambda_j$ gives:

$$\frac{q}{1 + e^\rho \bar{\lambda}} \leq \text{redf}(\rho).$$

This allows us to update ρ_{\min}^* , and in the end, we have:

$$\begin{aligned} \rho_{\min}^* &= \log \left(\frac{\kappa}{(1 - \kappa)\bar{\lambda}} \right), \\ \rho_{\max}^* &= \log \left(\frac{1 - \kappa}{\kappa \lambda_q} \right). \end{aligned} \quad (9)$$

At first glance, it appears that we still need all eigenvalues $(\lambda_j)_1^q$ in order to compute their mean $\bar{\lambda}$. But observing that these eigenvalues add up to:

$$\begin{aligned} \sum_{j=1}^q \lambda_j &= \text{tr}(\mathbf{\Lambda}) = \text{tr}(\mathbf{U}\mathbf{\Lambda}\mathbf{U}^{-1}) \\ &= \text{tr}(\mathbf{E}\mathbf{E}^T) = \|\mathbf{E}\|_F^2, \end{aligned}$$

we readily have (at $O(p^2)$ costs):

$$\bar{\lambda} = \frac{1}{q} \sum_{j=1}^q \lambda_j = \frac{\|\mathbf{E}\|_F^2}{q}.$$

This leaves the minimum eigenvalue λ_q the only nontrivial quantity in (9). The next section gives computational details for λ_q , which remarkably involve $O(p^2)$ complexity only. As a result, the wider search interval $[\rho_{\min}^*, \rho_{\max}^*]$ is available at $O(p^2)$ costs, much cheaper than the $O(p^3)$ costs for computing the exact search interval $[\rho_{\min}, \rho_{\max}]$.

3.3 Computational Details

We now describe $O(p^2)$ algorithms for computing the maximum and the minimum eigenvalues, i.e., λ_1 and λ_q , to aid fast computation of $[\rho_{\min}^*, \rho_{\max}^*]$. Note that although λ_1 does not show up in (9), it is useful for assessing the credibility of the computed λ_q . In addition, we can work with $\mathbf{E}^T \mathbf{E}$ instead of $\mathbf{E}\mathbf{E}^T$. Recall that $(\lambda_j)_1^q$ are the positive eigenvalues of the $p \times p$ positive semi-definite matrix $\mathbf{E}\mathbf{E}^T$. In fact, they are also the eigenvalues of the $q \times q$ positive definite matrix $\mathbf{E}^T \mathbf{E}$. This can be proved by using the singular value decomposition of \mathbf{E} . So rigorously speaking, λ_q is the minimum eigenvalue of $\mathbf{E}^T \mathbf{E}$ not $\mathbf{E}\mathbf{E}^T$.

In general, given a positive definite matrix \mathbf{A} , we compute its maximum eigenvalue using power iteration and its minimum eigenvalue using inverse iteration. The two algorithms iteratively compute $\mathbf{A}\mathbf{v}$ and $\mathbf{A}^{-1}\mathbf{v}$, respectively. Unfortunately, the latter operation is as expensive as $O(p^3)$ for $\mathbf{A} = \mathbf{E}^T \mathbf{E}$ as it is a dense matrix. Therefore, directly applying inverse iteration for λ_q is as costly as computing all $(\lambda_j)_1^q$ via a full eigendecomposition, which is a bad idea.

To obtain λ_q at $O(p^2)$ costs, we need to exploit the following partitioning:

$$\mathbf{E} = \begin{bmatrix} \mathbf{E}_1 \\ \mathbf{E}_2 \end{bmatrix},$$

where \mathbf{E}_1 is a $q \times q$ lower triangular matrix and \mathbf{E}_2 is an $m \times q$ rectangular matrix. Below is a demonstration of such structure (with $p = 6$, $m = 2$ and $q = 4$), where ‘ \times ’ and ‘ \circ ’ denote the nonzero elements in \mathbf{E}_1 and \mathbf{E}_2 , respectively.

$$\begin{bmatrix} \times & & & & & \\ \times & \times & & & & \\ \times & \times & \times & & & \\ \times & \times & \times & \times & & \\ \hline \circ & \circ & \circ & \circ & & \\ \circ & \circ & \circ & \circ & & \end{bmatrix}$$

Note that such “trapezoidal” structure exclusively holds for the penalized B-splines family. It allows us to express \mathbf{A} as an update to $\mathbf{E}_1^T \mathbf{E}_1$:

$$\mathbf{A} = \mathbf{E}^T \mathbf{E} = \mathbf{E}_1^T \mathbf{E}_1 + \mathbf{E}_2^T \mathbf{E}_2.$$

Using Woodbury identity (Woodbury, 1950), we obtain an explicit inversion formula:

$$\begin{aligned} \mathbf{A}^{-1} &= (\mathbf{E}_1^T \mathbf{E}_1)^{-1} - \mathbf{F}(\mathbf{I} + \mathbf{R}^T \mathbf{R})^{-1} \mathbf{F}^T \\ &= (\mathbf{E}_1^T \mathbf{E}_1)^{-1} - \mathbf{F}(\mathbf{G}\mathbf{G}^T)^{-1} \mathbf{F}^T, \end{aligned}$$

where $\mathbf{R} = (\mathbf{E}_1^T)^{-1} \mathbf{E}_2^T$ and $\mathbf{F} = \mathbf{E}_1^{-1} \mathbf{R}$ are both $q \times m$ matrices, and \mathbf{G} is the lower triangular Cholesky factor of the $m \times m$ matrix $\mathbf{I} + \mathbf{R}^T \mathbf{R}$. This transform the computation of $\mathbf{A}^{-1}\mathbf{v}$ into solving triangular linear systems with respect to \mathbf{E}_1 , \mathbf{E}_1^T , \mathbf{G} and \mathbf{G}^T , which are very efficient. See Algorithm 2 for implementation details and a breakdown of computational complexity. The penalty order m is often very small (usually 1, 2 or 3) and the number of iterations till convergence is much smaller than

q , so the overall costs remains $O(q^2)$ in practice. Since $q = p - m \approx p$, we report this complexity as $O(p^2)$.

Algorithm 2 Compute the minimum eigenvalue λ_q of $\mathbf{A} = \mathbf{E}^T \mathbf{E}$. Lines 1 to 5 compute matrices for applying Woodbury identity. Line 6 starts inverse iteration. Lines 10 to 16 compute $\mathbf{u} = \mathbf{A}^{-1} \mathbf{v}$.

```

1:  $\mathbf{E} = \begin{bmatrix} \mathbf{E}_1 \\ \mathbf{E}_2 \end{bmatrix}$ 
2: solve  $\mathbf{E}_1^T \mathbf{R} = \mathbf{E}_2^T$  for  $\mathbf{R}$   $\triangleright O(mq^2)$ 
3: solve  $\mathbf{E}_1 \mathbf{F} = \mathbf{R}$  for  $\mathbf{F}$   $\triangleright O(mq^2)$ 
4:  $\mathbf{H} = \mathbf{I} + \mathbf{R}^T \mathbf{R}$   $\triangleright O(m^3)$ 
5: Cholesky factorization  $\mathbf{H} = \mathbf{G} \mathbf{G}^T$   $\triangleright O(m^3)$ 
6: initialize  $\mathbf{u}$  as a random vector  $\triangleright O(q)$ 
7:  $\lambda = 0$ 
8: loop
9:    $\mathbf{v} = \mathbf{u} / \|\mathbf{u}\|$   $\triangleright O(q)$ 
10:  solve  $\mathbf{E}_1^T \mathbf{a}_1 = \mathbf{v}$  for  $\mathbf{a}_1$   $\triangleright O(q^2)$ 
11:  solve  $\mathbf{E}_1 \mathbf{a}_2 = \mathbf{a}_1$  for  $\mathbf{a}_2$   $\triangleright O(q^2)$ 
12:   $\mathbf{c}_1 = \mathbf{F}^T \mathbf{v}$   $\triangleright O(qm)$ 
13:  solve  $\mathbf{G} \mathbf{b}_1 = \mathbf{c}_1$  for  $\mathbf{b}_1$   $\triangleright O(m^2)$ 
14:  solve  $\mathbf{G}^T \mathbf{b}_2 = \mathbf{b}_1$  for  $\mathbf{b}_2$   $\triangleright O(m^2)$ 
15:   $\mathbf{c}_2 = \mathbf{F} \mathbf{b}_2$   $\triangleright O(qm)$ 
16:   $\mathbf{u} = \mathbf{a}_2 - \mathbf{c}_2$   $\triangleright O(q)$ 
17:   $\tilde{\lambda} = \mathbf{v}^T \mathbf{u}$   $\triangleright O(q)$ 
18:  if  $\tilde{\lambda} < 0$  then
19:    Warning:  $\mathbf{E}^T \mathbf{E}$  is numerically singular!
20:     $\lambda_q = 0$ 
21:    break
22:  end if
23:  if  $|\tilde{\lambda} - \lambda| < \lambda 10^{-6}$  then
24:    break
25:  end if
26:   $\lambda = \tilde{\lambda}$ 
27: end loop
28:  $\lambda_q = 1/\lambda$ 
29: if  $\lambda_q < \lambda_1 \varepsilon$  then
30:   Warning:  $\mathbf{E}^T \mathbf{E}$  is numerically singular!
31:    $\lambda_q = \lambda_1 \varepsilon$ 
32: end if
33: return  $\lambda_q$ 

```

An important technical detail in Algorithm 2 is that it checks the credibility of the computed λ_q . Although $\mathbf{E}^T \mathbf{E}$ is positive definite, in finite precision arithmetic performed by our computers, it becomes numerically singular if λ_q/λ_1 is smaller than the machine precision ε (the largest positive number such that $1 + \varepsilon = 1$). On modern 64-bit

CPUs, this precision is about 1.11×10^{-16} . In case of numerical singularity, λ_q can not be accurately computed due to loss of significant digits and the output λ_q is fake. The best bet in this case, is to reset the computed λ_q to $\lambda_1 \varepsilon$ (see lines 29 to 31). Sometimes, $\tilde{\lambda}$ computed at line 17 can be negative. This is an early sign of singularity and we can immediately stop the iteration (see lines 18 to 22). These procedures are necessary safety measures, without which the computed λ_q will be too small and the derived ρ_{\max}^* will be too big, making the PLS problem (2) unsolvable. In short, Algorithm 2 helps determine a search interval $[\rho_{\min}^*, \rho_{\max}^*]$ that is both sufficiently wide and numerically safe for grid search.

We need to acquire the maximum eigenvalue λ_1 prior to Algorithm 2. The computation of λ_1 is less challenging. Even a direct application of power iteration by iteratively computing $\mathbf{E}^T(\mathbf{E} \mathbf{v})$ is good enough at $O(p^2)$ costs. But we can make it more efficient by exploiting the band sparsity behind the “factor form” (4) of matrix \mathbf{E} . See Algorithm 3 for details. The overall complexity is $O(p)$ in practice.

Algorithm 3 Compute the maximum eigenvalue λ_1 of $\mathbf{A} = \mathbf{E}^T \mathbf{E}$, exploiting the band sparsity of \mathbf{L} and \mathbf{D}_m^T in the “factor form” (4) of matrix \mathbf{E} . Lines 5 to 8 compute $\mathbf{u} = \mathbf{A} \mathbf{v}$.

```

1: initialize  $\mathbf{u}$  as a random vector  $\triangleright O(q)$ 
2:  $\lambda = 0$ 
3: loop
4:    $\mathbf{v} = \mathbf{u} / \|\mathbf{u}\|$   $\triangleright O(q)$ 
5:    $\mathbf{b} = \mathbf{D}_m^T \mathbf{v}$   $\triangleright O(p)$ 
6:   solve  $\mathbf{L} \mathbf{a}_1 = \mathbf{b}$  for  $\mathbf{a}_1$   $\triangleright O(p)$ 
7:   solve  $\mathbf{L}^T \mathbf{a}_2 = \mathbf{a}_1$  for  $\mathbf{a}_2$   $\triangleright O(p)$ 
8:    $\mathbf{u} = \mathbf{D}_m \mathbf{a}_2$   $\triangleright O(p)$ 
9:    $\tilde{\lambda} = \mathbf{v}^T \mathbf{u}$   $\triangleright O(q)$ 
10:  if  $|\tilde{\lambda} - \lambda| < \lambda 10^{-6}$  then
11:    break
12:  end if
13:   $\lambda = \tilde{\lambda}$ 
14: end loop
15: return  $\lambda$ 

```

3.4 An Illustration of the Intervals

We now illustrate search intervals $[\rho_{\min}, \rho_{\max}]$ and $[\rho_{\min}^*, \rho_{\max}^*]$ through a simple example. We set up p

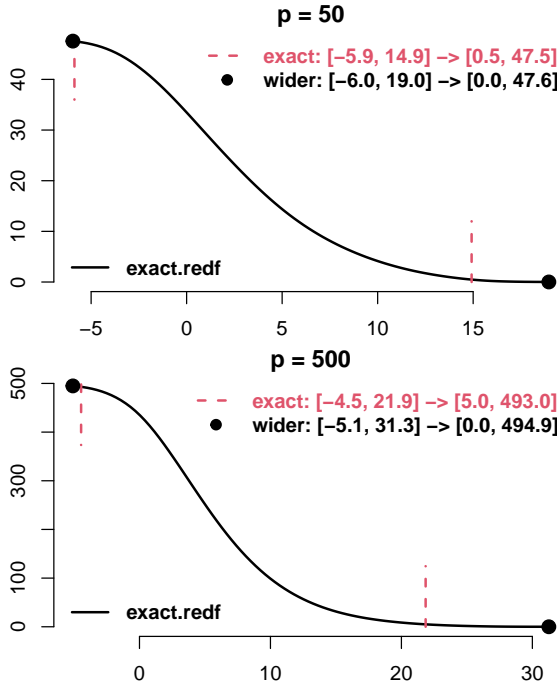


Fig. 2 An example of $\text{redf}(\rho)$ curve for p cubic B-splines ($d = 4$) on unevenly spaced knots, penalized by a 2nd order general difference penalty. The black dots (ρ_{\min}^* and ρ_{\max}^*) lie beyond the red dashed lines (ρ_{\min} and ρ_{\max}) on both ends, implying that $[\rho_{\min}^*, \rho_{\max}^*]$ is wider than $[\rho_{\min}, \rho_{\max}]$. The text (with numbers rounded to 1 decimal places) state the actual mapping from ρ range to redf range.

cubic B-splines ($d = 4$) on unevenly spaced knots and penalize them by a 2nd order general difference penalty ($m = 2$). We generate 10 uniformly distributed x values between every two adjacent knots and construct the design matrix \mathbf{B} at those locations. Figure 2 illustrates the resulting $\text{redf}(\rho)$ for $p = 50$ and $p = 500$. The nominal mapping from ρ range to redf range is $(-\infty, +\infty) \rightarrow [0, q]$ and here we have $q = p - 2$. For the exact interval, the mapping is $[\rho_{\min}, \rho_{\max}] \rightarrow [0.01q, 0.99q]$. The wider interval $[\rho_{\min}^*, \rho_{\max}^*]$ is mapped to a wider range than $[0.01q, 0.99q]$.

Our intervals are independent of y values and smoothness selection criteria. To illustrate this, we further simulate two sets of y values for the $p = 50$ case and choose the optimal ρ by minimizing GCV or maximizing REML. Figure 3 shows that while the two datasets produce different GCV or REML curves, they share the same search interval for ρ . (Note that in this Figure, both GCV and REML choose similar optimal ρ values in each example,

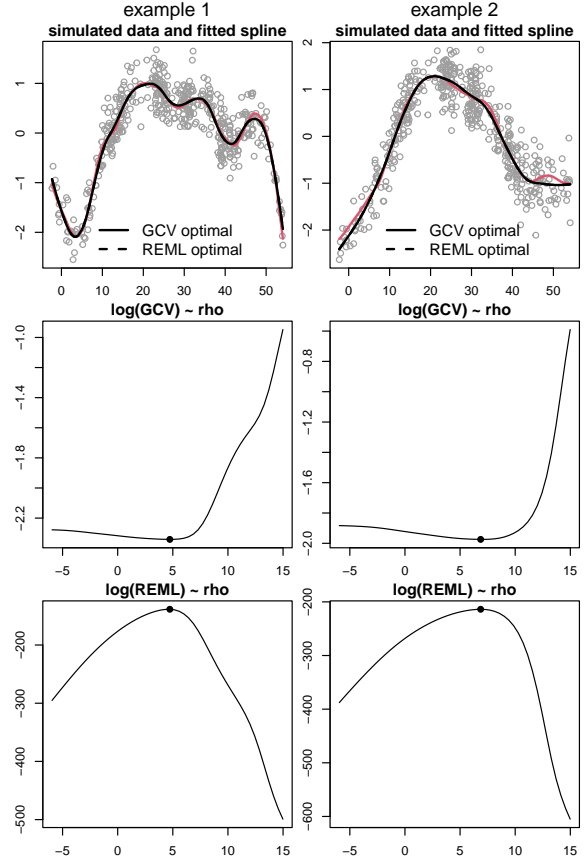


Fig. 3 Two sets of y values are simulated and smoothed for the $p = 50$ case in Figure 2. They yield different GCV or REML curves, but share the same search interval for ρ . In row 1, red curves are the true functions and black curves are the optimal spline fit.

leading to indistinguishable fit. This is not always true. See Section 5.)

3.5 Heuristic Improvement

Let's take a second look at Figure 2. As the black circle on the right end is far off the red dashed line, ρ_{\max}^* is a loose upper bound. Moreover, the bigger p is, the looser it is. We now use some heuristics to find a tighter upper bound. Specifically, we seek approximated eigenvalues $(\hat{\lambda}_j)_1^q$ such that $\hat{\lambda}_1 = \lambda_1$, $\hat{\lambda}_q = \lambda_q$ and $\sum_{j=1}^q \hat{\lambda}_j = q\bar{\lambda}$. Then, replacing λ_j by $\hat{\lambda}_j$ in (6) gives an approximated redf , to which we can apply method in Section 3.1 to obtain an “exact” search interval $[\hat{\rho}_{\min}, \hat{\rho}_{\max}]$. We are most interested in $\hat{\rho}_{\max}$, because empirically, it is tighter than ρ_{\max}^* , so we can narrow the search interval

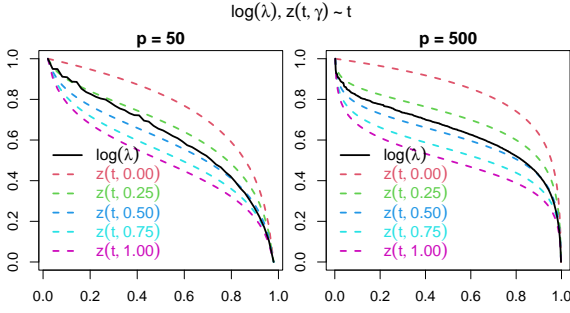


Fig. 4 The asymptotic decay pattern (red dashed) often does not reflect the actual decay pattern (black solid) of $\log(\lambda_j)$, because the first few eigenvalues may drop faster. Empirically, the actual decay is like an “S”-shaped curve $z(t_j, \gamma)$ and we can tweak γ value to make it similar (but not identical) to $\log(\lambda_j)$.

$[\rho_{\min}^*, \rho_{\max}^*]$ to $[\hat{\rho}_{\min}^*, \hat{\rho}_{\max}^*]$. We hereafter call $\hat{\rho}_{\max}$ the heuristic upper bound.

For reasonable approximation, knowledge on λ_j ’s decay pattern is useful. Recently, Xiao (2019, Lemma 5.1) established an asymptotic decay rate between $O((1 - \frac{j}{q+m})^{2m})$ and $O((1 - \frac{j+m}{q+m})^{2m})$ (Note: Xiao arranged $(\lambda_j)_1^q$ in ascending order so the Lemma states $O((\frac{j}{q+m})^{2m})$ and $O((\frac{j+m}{q+m})^{2m})$). So roughly speaking, $\log(\lambda_j)$ tends to decay along $z_j = \log(1 - t_j)$, where $t_j = j/(q+1)$. In practice however, we observed that the first few eigenvalues often drop faster, while the decay of the remaining eigenvalues well follows the theory. Empirically, the actual decay resembles an “S”-shaped curve:

$$z_j = z(t_j, \gamma) = \log(1 - t_j) + \gamma \log(1/t_j),$$

where $\gamma \in [0, 1]$ is a shape parameter. For example, Figure 4 illustrates the decay of $\log(\lambda_j)$ against t_j for the examples in the previous section. The fast decay of the first few eigenvalues and the resulting “S”-shaped curve are most noticeable for $p = 500$. The Figure also plots $z(t_j, \gamma)$ for various γ values and it appears that we can tweak γ value to make z_j similar to $\log(\lambda_j)$. Note that both $\log(\lambda_j)$ and z_j are transformed to $[0, 1]$ to ease shape comparison. Besides, $z(t_j, 0)$ is the asymptotic decay pattern and $z(t_j, 1)$ is the quantile of logistic distribution.

It is generally not possible to tweak γ value to make z_j identical to $\log(\lambda_j)$, so we instead model $\log(\lambda_j)$ as a function of z_j , i.e., $\log(\hat{\lambda}_j) = Q(z_j)$. For convenience, let $a = \log(\lambda_q)$, $b = \log(\lambda_1)$ and we transform $z_j \leftarrow (z_j - z_q)/(z_1 - z_q)$ so that z_j always ranges from 1 to 0. As we require $\hat{\lambda}_q = \lambda_q$

and $\hat{\lambda}_1 = \lambda_1$, the function must satisfy $Q(0) = a$ and $Q(1) = b$. To be able to determine $Q(z_j)$ with the last constraint $\sum_{j=1}^q \hat{\lambda}_j = q\bar{\lambda}$, we can only parameterize the function with one unknown. We now denote this function by $Q(z_j, \alpha)$ and suggest two parametrizations that prove to work well in practice. The first one is a quadratic polynomial:

$$Q_1(z_j, \alpha) = a + (b - a)z_j + \alpha(z_j^2 - z_j).$$

It is convex and monotonically increasing when $\alpha \in [0, b - a]$. The second one is a cubic polynomial:

$$\begin{aligned} Q_2(z_j, \alpha) = & [c_0(z_j) + c_2(z_j)]a + \\ & [c_2(z_j) + c_3(z_j)]b + \\ & [c_1(z_j) - c_2(z_j)]\alpha, \end{aligned}$$

represented using cubic Bernstein polynomials:

$$\begin{aligned} c_0(z_j) &= (1 - z_j)^3, & c_1(z_j) &= 3z_j(1 - z_j)^2, \\ c_2(z_j) &= 3z_j^2(1 - z_j), & c_3(z_j) &= z_j^3. \end{aligned}$$

It is an “S”-shaped curve and if $\alpha \in [a, (2a + b)/3]$, it is monotonically increasing, concave on $[0, 0.5]$ and convex on $[0.5, 1]$. See Figure 5 for what the two functions look like as α varies. To facilitate computation, we write both cases as:

$$\log(\hat{\lambda}_j) = Q(z_j, \alpha) = \theta_j + h_j \alpha, \quad \alpha \in [\alpha_l, \alpha_r].$$

Finding α such that $\sum_{j=1}^q \hat{\lambda}_j = q\bar{\lambda}$ is equivalent to finding the root of $g(\alpha) = \sum_{j=1}^q \exp(\theta_j + h_j \alpha) - q\bar{\lambda}$. As $g(\alpha)$ is differentiable, we use Newton’s method (see Algorithm 1) for this task. Note that a root exists in $[\alpha_l, \alpha_r]$ if and only if $g(\alpha_l) \cdot g(\alpha_r) \leq 0$. Therefore, we are not able to obtain approximated eigenvalues $(\hat{\lambda}_j)_1^q$ if this condition does not hold. Intuitively, the condition is met if $\log(\lambda_j)$, when sketched against z_j , largely lies on the “paths” of $Q(z_j, \alpha)$ as α varies (see Figure 5). This in turn implies that γ value should be properly chosen for $z_j = z(t_j, \gamma)$. For example, Figure 5 shows that $\gamma = 0.1$ is good for $Q_1(z_j, \alpha)$ but not for $Q_2(z_j, \alpha)$, whereas $\gamma = 0.45$ is good for $Q_2(z_j, \alpha)$ but not for $Q_1(z_j, \alpha)$.

In reality, we don’t know what γ value is good in advance, so a screening over $[0, 1]$ is needed, and for each trial γ value, we attempt both $Q_1(z_j, \alpha)$ and $Q_2(z_j, \alpha)$ (see Algorithm 4). We might have several successful approximations so we take their

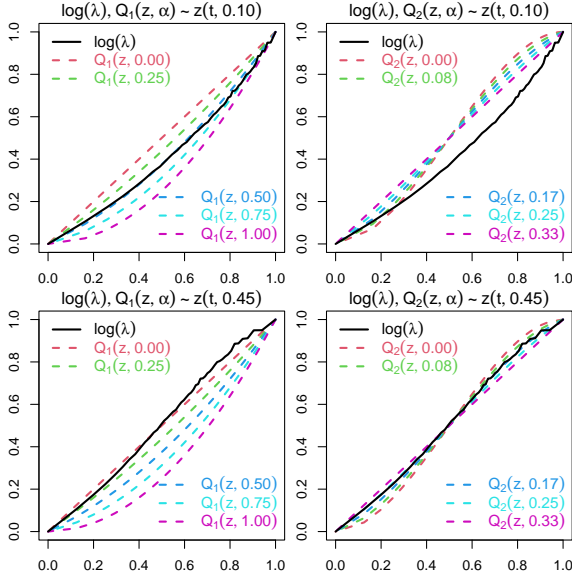


Fig. 5 We can approximate $\log(\lambda)$ by $\log(\hat{\lambda}_j) = Q(z_j, \alpha)$, if γ value is properly chosen for $z_j = z(t_j, \gamma)$ such that $\log(\lambda_j)$ (sketched against z_j) largely lies on the “paths” of $Q(z_j, \alpha)$ as α varies. In this example (the $p = 50$ case in Figure 4), $\gamma = 0.1$ is good for $Q_1(z_j, \alpha)$ but not for $Q_2(z_j, \alpha)$, whereas $\gamma = 0.45$ is good for $Q_2(z_j, \alpha)$ but not for $Q_1(z_j, \alpha)$.

average for the final $(\hat{\lambda}_j)_1^q$. Figure 6 shows $\log(\lambda_j)$ and $\log(\hat{\lambda}_j)$ (both transformed to $[0, 1]$) for the examples demonstrated through Figures 2 to 5. The approximation is almost perfect for small p (which is not surprising because smaller p means fewer eigenvalues to guess). As p increases, the approximation starts to deviate from the truth but is still accurate on both ends (which is important since the quality of heuristic bounds mainly relies on good approximation to extreme eigenvalues). Figure 7 displays the approximated redf and the heuristic upper bound $\hat{\rho}_{\max}$ (on top of Figure 2). Clearly, $\hat{\rho}_{\max}$ is closer to ρ_{\max} than ρ_{\max}^* and hence a tighter upper bound.

Algorithm 4 is very efficient at $O(q)$ costs as it only performs simple vector and scalar operations, so the complexity for finding the search interval $[\rho_{\min}^*, \hat{\rho}_{\max}]$ remains $O(p^2)$. Sometimes, it may fail to approximate eigenvalues so that the heuristic upper bound $\hat{\rho}_{\max}$ is not available and we have to stick to ρ_{\max}^* . It does not often happen, but in principle, the chance of failure can be further reduced by adding more flexibility to the heuristic. For example, we may introduce a new parameter $\nu \geq 1$ to model the “S”-shaped decay pattern as

Algorithm 4 Approximate eigenvalues of $\mathbf{E}^T \mathbf{E}$.

Input: (i) q , number of eigenvalues, (ii) λ_1, λ_q and $\bar{\lambda}$, max/min/mean eigenvalues. Quantities with subscript j are calculated for $j = 1, 2, \dots, q$. For the input of Algorithm 1, use $(\alpha_l + \alpha_r)/2$ for the initial value and choose $\delta_{\max} = (\alpha_r - \alpha_l)/4$.

```

1:  $a = \log(\lambda_q)$ ,  $b = \log(\lambda_1)$ 
2:  $t_j = j/(q+1)$ 
3:  $\hat{\lambda}_j = 0$  ▷ initialize approximation
4:  $N = 0$  ▷ number of successes
5: for  $\gamma = 0, 0.05, 0.10, \dots, 1$  do
6:    $z'_j = \log(1 - t_j) - \gamma \log(t_j)$  ▷ try  $z(t_j, \gamma)$ 
7:    $z_j = (z'_j - z'_q)/(z'_1 - z'_q)$ 
8:    $\theta_j = a + (b - a)z_j$  ▷ try  $Q_1(z_j, \alpha)$ 
9:    $h_j = z_j^2 - z_j$ 
10:   $\alpha_l = 0$ ,  $\alpha_r = b - a$ 
11:  if  $g(\alpha_l)g(\alpha_r) \leq 0$  then
12:    find root  $\alpha$  of  $g(\alpha)$  using Algorithm 1
13:     $N = N + 1$ 
14:     $\hat{\lambda}_j = \hat{\lambda}_j + \exp(\theta_j + \alpha h_j)$ 
15:  end if
16:   $c_{0j} = (1 - z_j)^3$  ▷ try  $Q_2(z_j, \alpha)$ 
17:   $c_{1j} = 3z_j(1 - z_j)^2$ 
18:   $c_{2j} = 3z_j^2(1 - z_j)$ 
19:   $c_{3j} = z_j^3$ 
20:   $\theta_j = a(c_{0j} + c_{2j}) + b(c_{2j} + c_{3j})$ 
21:   $h_j = c_{1j} - c_{2j}$ 
22:   $\alpha_l = a$ ,  $\alpha_r = (2a + b)/3$ 
23:  if  $g(\alpha_l)g(\alpha_r) \leq 0$  then
24:    find root  $\alpha$  of  $g(\alpha)$  using Algorithm 1
25:     $N = N + 1$ 
26:     $\hat{\lambda}_j = \hat{\lambda}_j + \exp(\theta_j + \alpha h_j)$ 
27:  end if
28: end for
29: if  $N > 0$  then ▷ average over successes
30:    $\hat{\lambda}_j = \hat{\lambda}_j / N$ 
31: else
32:   Warning: unable to approximate  $\lambda_j$ 
33: end if
34: return  $\lambda_j$ 
```

$z_j = z(t_j, \gamma, \nu) = \log(1 - t_j) + \gamma[\log(1/t_j)]^\nu$, which allows the first few eigenvalues to drop even faster. We may also propose $Q(z_j, \alpha)$ of new parametric forms. In short, Algorithm 4 is easily extensible for improvement.

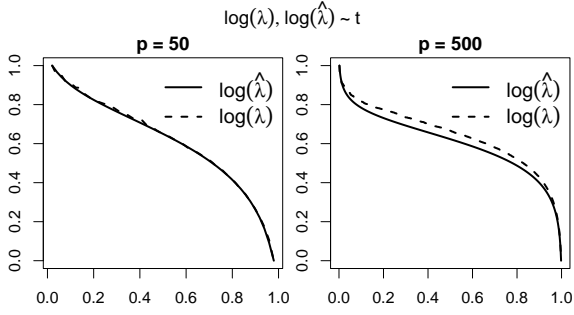


Fig. 6 Log eigenvalues $\log(\lambda_j)$ (solid) and their heuristic approximation $\log(\hat{\lambda}_j)$ (dashed) against t_j .

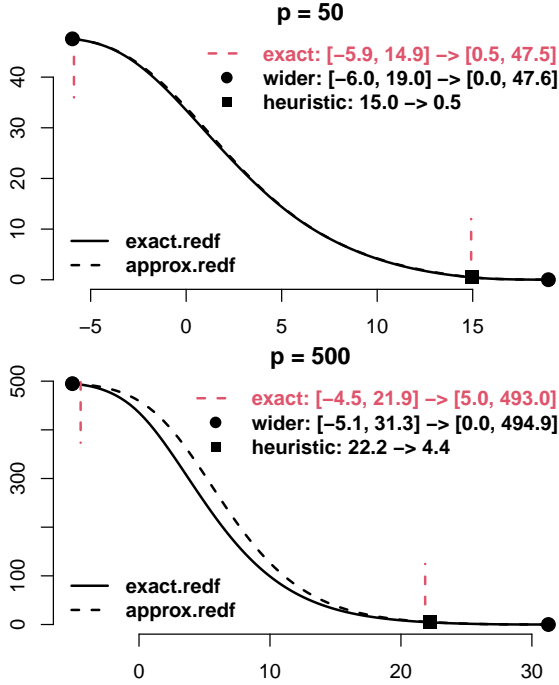


Fig. 7 Approximated $\text{redf}(\rho)$ (black dashed) and heuristic upper bound $\hat{\rho}_{\max}$ (black square). This Figure enhances Figure 2. Key message: $\hat{\rho}_{\max}$ is closer to ρ_{\max} (red dashed) than ρ_{\max}^* (black circle), hence a tighter upper bound.

3.6 Computation Time

We have developed two strategies to determine an appropriate search interval for ρ . We prefer the wider interval $[\rho_{\min}^*, \rho_{\max}^*]$ (or $[\rho_{\min}^*, \hat{\rho}_{\max}]$ if the heuristic upper bound $\hat{\rho}_{\max}$ is available) to the exact interval $[\rho_{\min}, \rho_{\max}]$ as its $O(p^2)$ costs is more affordable compared with the $O(Np^2)$ costs for solving PLS over N trial ρ values; otherwise, the $O(p^3)$ costs for computing the exact interval is too expensive for penalized B-splines. Table 1 reports the actual runtime of these computation

Table 1 Runtime (in seconds (s) or milliseconds (1ms = 0.001s)) of different computational tasks for growing p , on an Intel i5-8250U CPU @ 1.60GHz.

p	500	1000	1500	2000
$\rho_{\min}^*, \rho_{\max}^*, \hat{\rho}_{\max}$	4.74ms	0.02s	0.07s	0.15s
ρ_{\min}, ρ_{\max}	156.50ms	1.85s	7.48s	17.37s
PLS ($N = 20$)	58.30ms	0.25s	0.58s	1.00s

Table 2 The 8 scenarios for simulations

	derivative penalty	equidistant knots	weighted data
1	FALSE	FALSE	FALSE
2	TRUE	FALSE	FALSE
3	FALSE	TRUE	FALSE
4	TRUE	TRUE	FALSE
5	FALSE	FALSE	TRUE
6	TRUE	FALSE	TRUE
7	FALSE	TRUE	TRUE
8	TRUE	TRUE	TRUE

tasks for increasing p , well reflecting the practical impact of computational complexity.

4 Simulation Studies

Search intervals $[\rho_{\min}, \rho_{\max}]$ and $[\rho_{\min}^*, \rho_{\max}^*]$ have known property, because by construction, there are (taking $\kappa = 0.01$):

$$\begin{aligned} \rho_{\min}^* &\leq \rho_{\min}, & \text{redf}(\rho_{\min}^*) &\geq \text{redf}(\rho_{\min}) = 0.99q \\ \rho_{\max}^* &\geq \rho_{\max}, & \text{redf}(\rho_{\max}^*) &\leq \text{redf}(\rho_{\max}) = 0.01q. \end{aligned}$$

But $\hat{\rho}_{\max}$ is based on heuristic approximation and has unclear theoretical behavior. We expect it to be a tighter upper bound than ρ_{\max}^* , in the sense that it is closer to ρ_{\max} and ideally, $\rho_{\max} \leq \hat{\rho}_{\max} \leq \rho_{\max}^*$. This is supported by Figure 7, but we still need extensive simulations to be confident about this in general.

For comprehensiveness, we experiment every possible setup for penalized B-splines that affects $\text{redf}(\rho)$. The placement of equidistant or unevenly spaced knots produces different \mathbf{B} . The choice of difference or derivative penalty gives different \mathbf{D}_m . We also consider weighted data where (x_i, y_i) has weight w_i . This leads to a penalized weighted least squares problem (PWLS) that can be transformed to a PLS problem by absorbing weights into \mathbf{B} : $\mathbf{B} \leftarrow \mathbf{W}^{1/2} \mathbf{B}$, where \mathbf{W} is a diagonal matrix with element $W_{ii} = w_i$. Altogether, we have 8 scenarios (see Table 2).

Here are more implementation details for our simulations. To construct p order- d B-splines, we

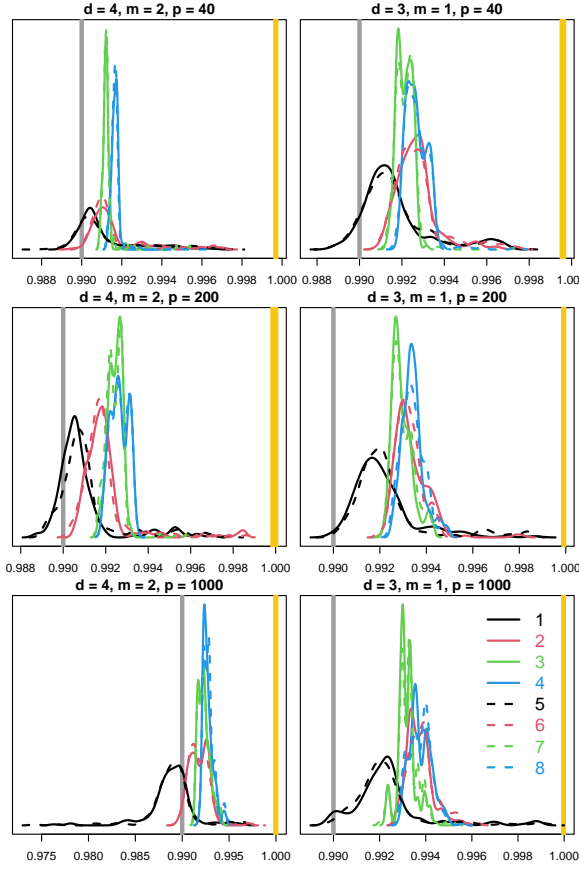


Fig. 8 Estimated probability density function of $P(\hat{\rho}_{\max})$, i.e., the proportion of $[0, q]$ covered by $[\text{redf}(\hat{\rho}_{\max}), q]$. If $\rho_{\max} \leq \hat{\rho}_{\max} \leq \rho_{\max}^*$, then the density curve lies between 0.99 (gray line) and $P(\rho_{\max}^*)$ (yellow line). Numbers 1 to 8 refer to the scenarios in Table 2.

need to place $p + d$ knots $(\xi_k)_1^{p+d}$. For equidistant knots, we let $\xi_k = k$. For unevenly spaced knots, we take $\xi_k \sim N(k, [(p + d)/10]^2)$. We generate 10 uniformly distributed x values between every two nearby knots for constructing the design matrix \mathbf{B} . To compute \mathbf{D}_m , we use `gpls::SparseD`. When data are weighted, we generate random weights from $\text{Beta}(3, 3)$ distribution. We will test different (d, m) pairs for growing p , with 8 scenarios in each case.

In principle, we want to run an experiment, say 200 times, and see how $\hat{\rho}_{\max}$ is distributed relative to ρ_{\max} and ρ_{\max}^* . But as none of these quantities stays fixed between runs, visualization is not easy. Let's switch to redf -oriented thinking and compare the proportion of $[0, q]$ covered by $[\text{redf}(\rho_{\max}), q]$,

$[\text{redf}(\hat{\rho}_{\max}), q]$ and $[\text{redf}(\rho_{\max}^*), q]$, i.e.,

$$P(\rho_{\max}) = 1 - \text{redf}(\rho_{\max})/q = 0.99,$$

$$P(\hat{\rho}_{\max}) = 1 - \text{redf}(\hat{\rho}_{\max})/q,$$

$$P(\rho_{\max}^*) = 1 - \text{redf}(\rho_{\max}^*)/q.$$

Because $\text{redf}(\rho)$ is decreasing, if we expect $\rho_{\max} \leq \hat{\rho}_{\max} \leq \rho_{\max}^*$, we should observe $0.99 \leq P(\hat{\rho}_{\max}) \leq P(\rho_{\max}^*)$. Interestingly, simulations show that the variance of $P(\rho_{\max}^*)$ is so low that its probability density function almost degenerates to a vertical line through its mean. This implies that we need to check if the density curve of $P(\hat{\rho}_{\max})$ lies between two vertical lines. Figure 8 illustrates simulation results for cubic splines with a 2nd order penalty and quadratic splines with a 1st order penalty as p grows. They look satisfying except for scenarios 1 and 5. In these cases, a non-negligible proportion of the density curve breaches 0.99, so we will get $\hat{\rho}_{\max} < \rho_{\max}$ occasionally. Strictly speaking, the resulting search interval $[\rho_{\min}^*, \hat{\rho}_{\max}]$ is narrower than $[\rho_{\min}, \rho_{\max}]$ and hence undesirable. However, it is wide enough in practice, as the corresponding redf range still covers a significant proportion of $[0, q]$ (see the numbers labeled along the x-axis of each graph in the Figure). So empirically, $\hat{\rho}_{\max}$ is a tight upper bound for grid search.

5 Application

In this section, we revisit the COVID-19 example in Introduction. To stress that our search interval $[\rho_{\min}^*, \hat{\rho}_{\max}]$ is criterion-independent, we illustrate smoothness selection using both GCV and REML.

The Finland dataset reports new deaths on 408 out of 542 days from 2020-09-01 to 2022-03-01. The Netherlands dataset reports new cases on 181 out of 182 days from 2021-09-01 to 2022-03-01. Let n be the number of data. For smoothing we set up cubic B-splines on $n/4$ knots placed at equal quantiles of the reporting days, and penalize them by a 2nd order general difference penalty. For the Finland example, our computed search interval is $[\rho_{\min}^*, \hat{\rho}_{\max}] = [-6.15, 14.93]$ (with $\rho_{\max}^* = 20.25$). For the Netherlands example, the search interval is $[\rho_{\min}^*, \hat{\rho}_{\max}] = [-6.26, 13.05]$ (with $\rho_{\max}^* = 16.97$). Figure 9 sketches $\text{edf}(\rho)$, $\text{GCV}(\rho)$ and $\text{REML}(\rho)$ on the search intervals. For both examples, GCV has a local minimum and a global minimum (see Figure 1 for a zoomed-in display), whereas REML

has a single maximum. In addition, the optimal ρ value chosen by REML is bigger than that selected by GCV, yielding a smoother yet more plausible fit. In fact, theoretical properties of both criteria have been well studied by [Reiss and Ogden \(2009\)](#). In short, GCV is more likely to have multiple local extrema. It is also more likely to underestimate the optimal ρ and cause overfitting. Thus, REML is superior to GCV for smoothness selection. But anyway, the focus here is not to discuss the choice of selection criterion, but to demonstrate that our automatic search interval for ρ is wide enough for exploring any criterion.

The edf curves in Figure 9 show that more than half of the B-spline coefficients are suppressed by the penalty in the optimal fit. In the Finland case, the maximum possible edf in Figure 9 is 106, but the optimal edf (whether 43.1 or 12.6) is less than half of that. To avoid such waste, we can halve the number of knots, i.e., place $n/8$ knots. This alters the design matrix, the penalty matrix and hence $\text{edf}(\rho)$, so the search interval needs be recomputed. The new interval is $[\rho_{\min}^*, \hat{\rho}_{\max}] = [-6.16, 13.30]$ (with $\rho_{\max}^* = 17.47$) for the Finland example and $[\rho_{\min}^*, \hat{\rho}_{\max}] = [-6.43, 11.51]$ (with $\rho_{\max}^* = 14.66$) for the Netherlands example. Figure 10 sketches $\text{edf}(\rho)$, $\text{GCV}(\rho)$ and $\text{REML}(\rho)$ on their new range. Interestingly, $\text{GCV}(\rho)$ no longer has a second local minimum. The Figure does not further show the fitted splines because they are almost identical to their counterparts in Figure 9.

6 Conclusion

We developed automatic algorithms to determine a search interval for smoothing parameter ρ in penalized B-splines, so that practitioners no longer need to obtain it by trial and error prior to grid search. Our automatic search interval has four advantages. (i) It gives a safe ρ range where the penalized least squares problem is numerically solvable. (ii) It is criterion-independent so that different criteria can be explored on the same ρ range. (iii) It is wide enough to contain the global extremum of any smoothness selection criterion, so for example, the global minimum of GCV and the global maximum of REML can both be found. (iv) It is computationally cheap compared with grid search, so in practice it carries no extra costs. Note that although our interval is most relevant to grid search, it is also helpful for gradient descent

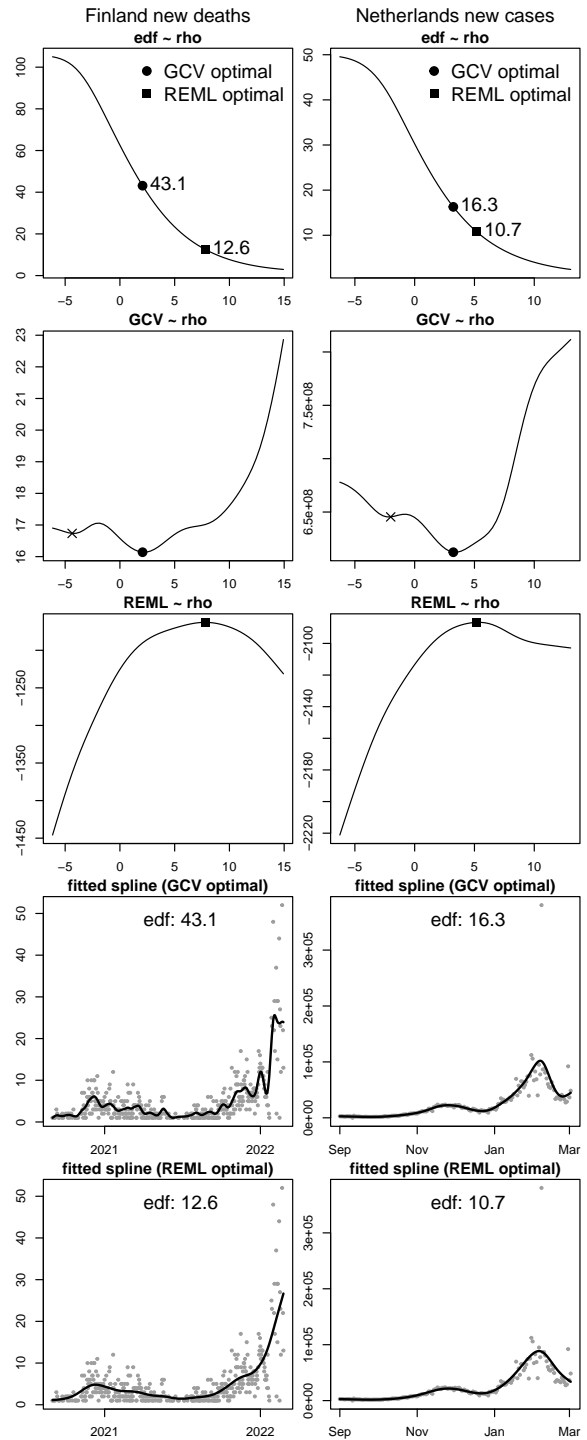


Fig. 9 Smoothing daily COVID-19 data in Finland ($n = 408$ data; displayed in column 1) and Netherlands ($n = 182$ data; displayed in column 2). A cubic general P-spline with $n/4$ knots and a 2nd order difference penalty is used for smoothing. For both examples, the optimal ρ value chosen by REML is bigger than that selected by GCV, resulting in a smoother yet more plausible fit.

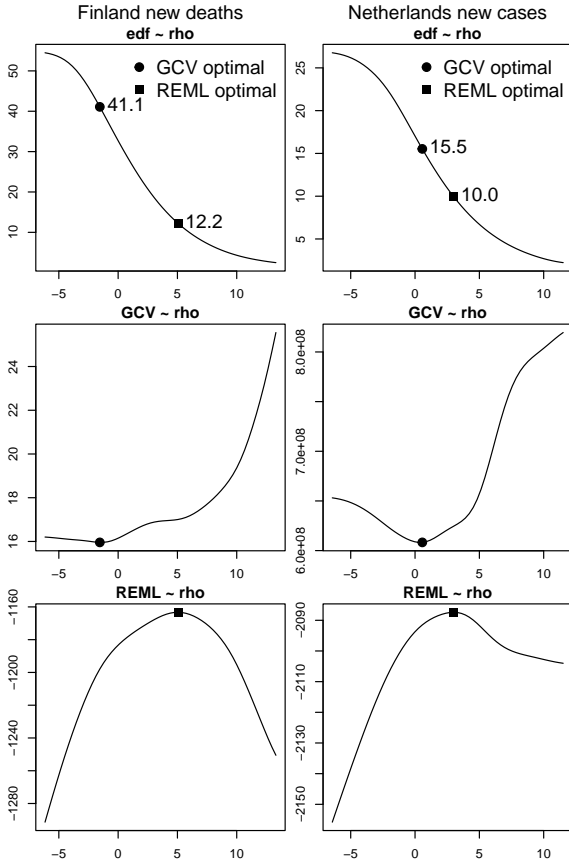


Fig. 10 The altered $\text{edf}(\rho)$, $\text{GCV}(\rho)$ and $\text{REML}(\rho)$ after we halve the number of knots in the COVID-19 smoothing example. Interestingly, GCV no longer has a second local minimum.

and Newton's method. Specifically, the midpoint of the interval is a good initial ρ value. However, these methods are generally not as reliable as grid search, as they may converge to an undesired local minimum rather than the global minimum.

Our method can be applied to any penalized spline, but we have given penalized B-splines a special focus, because this is when it is difficult to develop algorithms to attain (iv). B-splines are sparse and their penalized least squares problem can be solved efficiently at $O(p^2)$ costs, so it is not computationally appealing to find an exact search interval through an eigendecomposition at $O(p^3)$ costs. We therefore turn to finding a wider search interval (with optional heuristic improvement) at $O(p^2)$ costs. However, for other types of penalized splines (1), at least one of \mathbf{B} and \mathbf{S} are dense matrices. Computing an exact search interval is now acceptable because it costs $O(p^3)$ to solve the

penalized least squares problem anyway. Note that we don't have matrix \mathbf{D}_m or \mathbf{E} in this situation, so we express matrix \mathbf{C} (see (5)) as:

$$\mathbf{C} = \mathbf{L}\mathbf{L}^T + e^\rho \mathbf{S} = \mathbf{L}[\mathbf{I} + e^\rho \mathbf{L}^{-1} \mathbf{S} (\mathbf{L}^{-1})^T] \mathbf{L}^T,$$

and compute the eigenvalues of $\mathbf{L}^{-1} \mathbf{S} (\mathbf{L}^{-1})^T$.

Our method is ready to use through function `gps2GS` in **R** package `gps` (\geq version 1.1). The function computes the automatic search interval and optionally solve the penalized least squares problem for a grid of ρ values. It may be embedded in other advanced statistical modeling methods that rely on penalized splines, like robust smoothing and generalized additive models.

Declarations

Funding. Zheyuan Li was supported by National Natural Science Foundation of China under Young Scientists Fund NSFC-12001166. Jiguo Cao was supported by Natural Sciences and Engineering Research Council of Canada under Discovery Grant 2018-06008.

Conflict of interest. The authors declare that they have no conflict of interest.

Code availability. The **R** code for this paper is available as a vignette at <https://github.com/ZheyuanLi/gps-vignettes/blob/main/gps2.pdf>.

Appendix A Examples of \mathbf{D}_m

Here are some example \mathbf{D}_m matrices for standard P-splines (SPS), O-splines (OS) and general P-splines (GPS). They are calculated using function `SparseD` from **R** package `gps`. For technical details on \mathbf{D}_m , see Li and Cao (2022a).

B-splines on equidistant knots can be used in SPS, GPS and OS, and in this case, SPS and GPS are equivalent. For example, for cubic B-splines on 10 equidistant knots from 0 to 1 (see Figure A1), we can use the 2nd order matrices below (numbers are rounded to 2 decimal places):

$$\mathbf{D}_2^{\text{sps/gps}} = \begin{bmatrix} 1 & -2 & 1 & & & \\ & 1 & -2 & 1 & & \\ & & 1 & -2 & 1 & \\ & & & 1 & -2 & 1 \end{bmatrix},$$

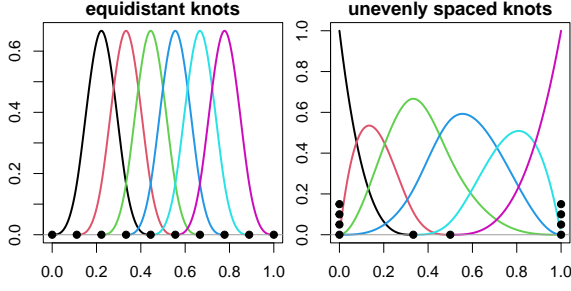


Fig. A1 Cubic B-splines on 10 equidistant knots and 10 unevenly spaced knots.

$$D_2^{\text{os}} = \begin{bmatrix} 0.19 & -0.29 & 0.00 & 0.10 & & \\ & 0.25 & -0.44 & 0.11 & 0.07 & \\ & & 0.26 & -0.45 & 0.12 & 0.07 \\ & & & 0.18 & -0.36 & 0.18 \end{bmatrix}.$$

B-splines on unevenly spaced knots can only be used in GPS and OS. For example, for cubic B-splines on 10 unevenly spaced knots 0, 0, 0, 0, $\frac{1}{3}$, $\frac{1}{2}$, 1, 1, 1, 1 (see Figure A1), we can use the 2nd order matrices below (numbers are rounded to 2 decimal places):

$$D_2^{\text{gps}} = \begin{bmatrix} 54 & -90 & 36 & & \\ & 24 & -36 & 12.0 & \\ & & 9 & -22.5 & 13.5 \\ & & & 18.0 & -42.0 & 24 \end{bmatrix},$$

$$D_2^{\text{os}} = \begin{bmatrix} 18 & -26.00 & 6.00 & 2.00 & & \\ & 8.94 & -12.75 & 2.80 & 1.01 & \\ & & 4.19 & -7.25 & -1.24 & 4.30 \\ & & & 6.60 & -15.41 & 8.81 \end{bmatrix}.$$

Appendix B REML

We now derive the restricted log-likelihood of ρ . For convenience, denote the PLS objective (2) by $\text{PLS}(\beta)$. It can be verified that:

$$\text{PLS}(\beta) = \text{PLS}(\hat{\beta}) + (\beta - \hat{\beta})^T C (\beta - \hat{\beta}).$$

The least squares term in $\text{PLS}(\beta)$ corresponds to the Gaussian likelihood:

$$\Pr(\mathbf{y}|\beta) = c_1 \cdot \exp \left\{ -\frac{\|\mathbf{y} - B\beta\|^2}{2\sigma^2} \right\},$$

with $c_1 = (2\pi\sigma^2)^{-n/2}$. In the Bayesian view, the wiggleness penalty $e^\rho \|\mathbf{D}_m \beta\|^2$ is a Gaussian prior:

$$\Pr(\beta) = c_2 \cdot \exp \left\{ -\frac{e^\rho \|\mathbf{D}_m \beta\|^2}{2\sigma^2} \right\},$$

with $c_2 = (2\pi\sigma^2)^{-(p-m)/2} \cdot e^{(p-m)\rho/2} \cdot |\mathbf{D}_m \mathbf{D}_m^T|^{1/2}$ where $|\mathbf{X}|$ denotes the determinant of \mathbf{X} . Then, the unnormalized posterior is:

$$\begin{aligned} \Pr(\mathbf{y}|\beta) \cdot \Pr(\beta) &= c_1 \cdot c_2 \cdot \exp \left\{ -\frac{\text{PLS}(\beta)}{2\sigma^2} \right\} \\ &= c_1 \cdot c_2 \cdot \exp \left\{ -\frac{\text{PLS}(\hat{\beta})}{2\sigma^2} \right\} \exp \left\{ -\frac{(\beta - \hat{\beta})^T C (\beta - \hat{\beta})}{2\sigma^2} \right\}. \end{aligned}$$

The restricted likelihood of hyperparameters ρ and σ^2 is:

$$\begin{aligned} L_r(\rho, \sigma^2) &= \int \Pr(\mathbf{y}|\beta) \cdot \Pr(\beta) \, d\beta \\ &= c_1 \cdot c_2 \cdot c_3 \cdot \exp \left\{ -\frac{\text{PLS}(\hat{\beta})}{2\sigma^2} \right\}, \end{aligned}$$

with

$$\begin{aligned} c_3 &= \int \exp \left\{ -\frac{(\beta - \hat{\beta})^T C (\beta - \hat{\beta})}{2\sigma^2} \right\} d\beta \\ &= (2\pi\sigma^2)^{p/2} \cdot |\mathbf{C}|^{-1/2}. \end{aligned}$$

Therefore, the restricted log-likelihood is:

$$\begin{aligned} l_r(\rho, \sigma^2) &= \log(c_1) + \log(c_2) + \log(c_3) - \frac{\text{PLS}(\hat{\beta})}{2\sigma^2} \\ &= \frac{1}{2} \log |\mathbf{D}_m \mathbf{D}_m^T| + \frac{n-m}{2} \rho - \frac{1}{2} \log |\mathbf{C}| - \\ &\quad \frac{n-m}{2} \log(2\pi\sigma^2) - \frac{\text{PLS}(\hat{\beta})}{2\sigma^2}. \end{aligned}$$

Replacing σ^2 by its Pearson estimate $\hat{\sigma}^2 = \frac{\|\mathbf{y} - \hat{\mathbf{y}}\|^2}{n - \text{edf}}$ gives a criterion function of ρ only:

$$\begin{aligned} \text{REML}(\rho) &= \frac{1}{2} \log |\mathbf{D}_m \mathbf{D}_m^T| + \frac{n-m}{2} \rho - \frac{1}{2} \log |\mathbf{C}| - \\ &\quad \frac{n-m}{2} \log(2\pi\hat{\sigma}^2) - \frac{\text{PLS}(\hat{\beta})}{2\hat{\sigma}^2}. \end{aligned}$$

Note that the last term can be expressed as:

$$\begin{aligned} \frac{\text{PLS}(\hat{\beta})}{2\hat{\sigma}^2} &= \frac{\|\mathbf{y} + B\hat{\beta}\|^2 + e^\rho \|\mathbf{D}_m \hat{\beta}\|^2}{2\hat{\sigma}^2} \\ &= \frac{\|\mathbf{y} - \hat{\mathbf{y}}\|^2 + e^\rho \|\mathbf{D}_m \hat{\beta}\|^2}{2\hat{\sigma}^2} \\ &= \frac{n - \text{edf}}{2} + \frac{e^\rho \|\mathbf{D}_m \hat{\beta}\|^2}{2\hat{\sigma}^2}. \end{aligned}$$

As a result, we have:

$$\begin{aligned} \text{REML}(\rho) &= \frac{1}{2} \log |\mathbf{D}_m \mathbf{D}_m^T| + \frac{n-m}{2} \rho - \frac{1}{2} \log |\mathbf{C}| - \\ &\quad \frac{n-m}{2} \log(2\pi\hat{\sigma}^2) - \frac{n - \text{edf}}{2} - \frac{e^\rho \|\mathbf{D}_m \hat{\beta}\|^2}{2\hat{\sigma}^2}. \end{aligned}$$

References

- Andrinopoulou ER, Eilers PHC, Takkenberg JJM, et al (2018) Improved dynamic predictions from joint models of longitudinal and survival data with time-varying effects using P-splines. *Biometrics* 74(2):685–693. <https://doi.org/10.1111/biom.12814>
- de Boor C (2001) A Practical Guide to Splines (Revised Edition), Applied Mathematical Sciences, vol 27. Springer New York
- Bremhorst V, Lambert P (2016) Flexible estimation in cure survival models using Bayesian P-splines. *Computational Statistics & Data Analysis* 93(SI):270–284. <https://doi.org/10.1016/j.csda.2014.05.009>
- Chen J, Ohlssen D, Zhou Y (2018) Functional mixed effects model for the analysis of dose-titration studies. *Statistics in Biopharmaceutical Research* 10(3):176–184. <https://doi.org/10.1080/19466315.2018.1458649>
- Demmler A, Reinsch C (1975) Oscillation matrices with spline smoothing. *Numerische Mathematik* 24(5):375–382. <https://doi.org/10.1007/BF01437406>
- Dreassi E, Ranalli MG, Salvati N (2014) Semiparametric M-quantile regression for count data. *Statistical Methods in Medical Research* 23(6):591–610. <https://doi.org/10.1177/0962280214536636>
- Eilers P, Marx B (2002) Generalized linear additive smooth structures. *Journal of Computational and Graphical Statistics* 11(4):758–783. <https://doi.org/10.1198/106186002844>
- Eilers PHC, Marx BD (1996) Flexible smoothing with B-splines and penalties. *Statistical Science* 11(2):89–102. <https://doi.org/10.1214/ss/1038425655>
- Franco-Villoria M, Scott M, Hoey T (2019) Spatiotemporal modeling of hydrological return levels: A quantile regression approach. *Environmetrics* 30(2, SI). <https://doi.org/10.1002/env.2522>
- Gijbels I, Ibrahim MA, Verhasselt A (2018) Testing the heteroscedastic error structure in quantile varying coefficient models. *Canadian Journal of Statistics* 46(2):246–264. <https://doi.org/10.1002/cjs.11346>
- Goicoa T, Adin A, Etxeberria J, et al (2019) Flexible Bayesian P-splines for smoothing age-specific spatio-temporal mortality patterns. *Statistical Methods in Medical Research* 28(2):384–403. <https://doi.org/10.1177/0962280217726802>
- Greco F, Ventrucci M, Castelli E (2018) P-spline smoothing for spatial data collected worldwide. *Spatial Statistics* 27:1–17. <https://doi.org/10.1016/j.spasta.2018.08.008>
- Hendrickx K, Janssen P, Verhasselt A (2018) Penalized spline estimation in varying coefficient models with censored data. *TEST* 27(4):871–895. <https://doi.org/10.1007/s11749-017-0574-y>
- Hernando Vanegas L, Paula GA (2016) An extension of log-symmetric regression models: R codes and applications. *Journal of Statistical Computation and Simulation* 86(9):1709–1735. <https://doi.org/10.1080/00949655.2015.1081689>
- Koehler M, Umlauf N, Beyerlein A, et al (2017) Flexible Bayesian additive joint models with an application to type 1 diabetes research. *Biometrical Journal* 59(6, SI):1144–1165. <https://doi.org/10.1002/bimj.201600224>
- Li Z, Cao J (2022a) General P-splines for non-uniform B-splines. Preprint at <https://arxiv.org/abs/2201.06808v2>
- Li Z, Cao J (2022b) gps: General P-Splines. URL <https://CRAN.R-project.org/package=gps>, R package version 1.1
- Minguez R, Basile R, Durban M (2020) An alternative semiparametric model for spatial panel data. *Statistical Methods and Applications* 29(4):669–708. <https://doi.org/10.1007/s10260-019-00492-8>

- Muggeo VMR, Torretta F, Eilers PHC, et al (2021) Multiple smoothing parameters selection in additive regression quantiles. *Statistical Modelling* 21(5):428–448. <https://doi.org/10.1177/1471082X20929802>
- Oliveira RA, Paula GA (2021) Additive models with autoregressive symmetric errors based on penalized regression splines. *Computational Statistics* 36(4):2435–2466. <https://doi.org/10.1007/s00180-021-01106-2>
- Orbe J, Virto J (2021) Selecting the smoothing parameter and knots for an extension of penalized splines to censored data. *Journal of Statistical Computation and Simulation* 91(14):2953–2985. <https://doi.org/10.1080/00949655.2021.1913737>
- Osorio F (2016) Influence diagnostics for robust P-splines using scale mixture of normal distributions. *Annals of the Institute of Statistical Mathematics* 68(3):589–619. <https://doi.org/10.1007/s10463-015-0506-0>
- O’Sullivan F (1986) A statistical perspective on ill-posed inverse problems. *Statistical Science* 1(4):502–518. <https://doi.org/10.1214/ss/1177013525>
- Reinsch CH (1967) Smoothing by spline functions. *Numerische Mathematik* 10(3):177–183. <https://doi.org/10.1007/BF02162161>
- Reinsch CH (1971) Smoothing by spline functions. II. *Numerische Mathematik* 16(5):451–454. <https://doi.org/10.1007/BF02169154>
- Reiss PT, Ogden RT (2009) Smoothing parameter selection for a class of semiparametric linear models. *Journal of the Royal Statistical Society: Series B (Statistical Methodology)* 71(2):505–523. <https://doi.org/10.1111/j.1467-9868.2008.00695.x>
- Ritchie H, Mathieu E, Rodés-Guirao L, et al (2020) Coronavirus Pandemic (COVID-19). *Our World in Data* URL <https://ourworldindata.org/coronavirus>
- Rodriguez-Alvarez MX, Boer MP, van Eeuwijk FA, et al (2018) Correcting for spatial heterogeneity in plant breeding experiments with P-splines. *Spatial Statistics* 23:52–71. <https://doi.org/10.1016/j.spasta.2017.10.003>
- Ruppert D, Wand MP, Carroll RJ (2003) *Semiparametric Regression*. Cambridge Series in Statistical and Probabilistic Mathematics, Cambridge University Press
- Spiegel E, Kneib T, Otto-Sobotka F (2019) Generalized additive models with flexible response functions. *Statistics and Computing* 29(1):123–138. <https://doi.org/10.1007/s11222-017-9799-6>
- Spiegel E, Kneib T, Otto-Sobotka F (2020) Spatio-temporal expectile regression models. *Statistical Modelling* 20(4):386–409. <https://doi.org/10.1177/1471082X19829945>
- Wahba G (1990) *Spline models for observational data*. Society for Industrial and Applied Mathematics
- Wang X, Roy V, Zhu Z (2018) A new algorithm to estimate monotone nonparametric link functions and a comparison with parametric approach. *Statistics and Computing* 28(5):1083–1094. <https://doi.org/10.1007/s11222-017-9781-3>
- Wood SN (2017) *Generalized Additive Models: An Introduction with R*, 2nd edn. Chapman and Hall
- Woodbury MA (1950) Inverting modified matrices. Tech. Rep. 42, Princeton University
- Xiao L (2019) Asymptotic theory of penalized splines. *Electronic Journal of Statistics* 13(1):747–794. <https://doi.org/10.1214/19-EJS1541>
- Yu Y, Wu C, Zhang Y (2017) Penalised spline estimation for generalised partially linear single-index models. *Statistics and Computing* 27(2):571–582. <https://doi.org/10.1007/s11222-016-9639-0>